Non-Hermitian Fabry-Pérot resonances in a *PT*-symmetric system

Ken Shobe

Department of Semiconductor Electronics and Integration Science, AdSM, Hiroshima University, 739-8530, Japan

Keiichi Kuramoto

Program of Electronic Devices and Systems, School of Engineering, Hiroshima University, 739-8527, Japan

Ken-Ichiro Imura ⓘ

Graduate School of Advanced Science and Engineering, Hiroshima University, 739-8530, Japan

Naomichi Hatano ⓘ

Institute of Industrial Science, The University of Tokyo, 277-8574, Japan

In non-Hermitian scattering problems, the behavior of the transmission probability is very different from its Hermitian counterpart; it can exceed unity or even be divergent, since the non-Hermiticity can add or remove the probability to and from the scattering system. In the present paper, we consider the scattering problem of a *PT*-symmetric potential, and we find a counterintuitive behavior. In the usual *PT*-symmetric non-Hermitian system, we would typically find stationary semi-Hermitian dynamics in a regime of weak non-Hermiticity but observe instability once the non-Hermiticity goes beyond an exceptional point. Here, in contrast, the behavior of the transmission probability is strongly non-Hermitian in the regime of weak non-Hermiticity with divergent peaks, while it is superficially Hermitian in the regime of strong non-Hermiticity, recovering the conventional Fabry-Pérot-type peak structure. We show that the unitarity of the *S*-matrix is generally broken in both of the regimes, but is recovered in the limit of infinitely strong non-Hermiticity.

I. INTRODUCTION

Non-Hermitian quantum mechanics has attracted a great deal of attention recently; for a recent review, see, e.g., Ref. [1]. Historically, it dates back to the mid-20th century, when nuclear physicists, particularly Feshbach, introduced the idea of optical potential [2–4] for the description of nuclear decay in terms of resonant states with complex eigenvalues in scattering theory. Feshbach later justified [5,6] the complexity of the optical potential by means of projection operators, which we can refer to as a theory of open quantum systems [7–10] in present-day terminology.

Interest in non-Hermitian systems was revived in the late 1990s. A tight-binding model with asymmetric hopping, namely an imaginary vector potential, was introduced in 1996 as an effective model of type-II superconductors, and it was connected to Anderson localization [11,12]. This stimulated the theory of non-Hermitian random matrices [13–15].

A model of an oscillator with parity-time (*PT*) symmetric nonharmonic potential was introduced in 1998 in order to replace the concept of Hermiticity as a condition for the reality of the energy eigenvalue [16,17]. This triggered experimental studies on various effectively *PT*-symmetric systems, mainly optical systems [18–25], and the last couple of years has seen an explosive development of study on non-Hermitian systems of various types. The study of *PT*-symmetric systems also motivated many researchers to generalize arguments on the symmetry and topology of Hermitian systems [26–29] to non-Hermitian ones. The non-Hermitian topological insulator has been studied both in *PT*-symmetric [27,30–34] and asymmetric hopping models [35–39].

However, a fully quantum-mechanical realization of *PT*-symmetric systems has only been partially achieved [40]. In the present paper, we solve the scattering problem of a *PT*-symmetric system shown in Fig. 1 from the perspective of finding a fully quantum-mechanical experimental situation for detecting signatures of *PT* symmetry and non-Hermiticity. The *PT*-symmetric potential may be materialized by attaching environmental systems of source and sink, as is suggested by the studies of optical potential.

A lesson that we can learn from the studies on nuclear physics performed in the 20th century is that the infinite space outside the scatterer in a typical potential scattering problem is in reality terminated by macroscopic neutron injectors and detectors. Condensed-matter physicists may be more familiar with the same concept in a different context of the Landauer formula [41]. The infinite leads substitute the macroscopic source and drain to measure the electronic conduction of a microscopic system. In this sense, any realistic experimental situations are open systems in which macroscopic probes may
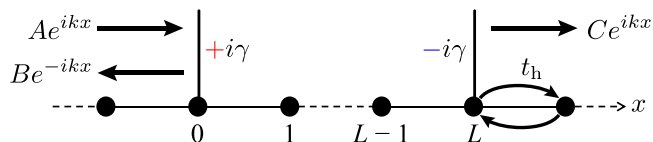
FIG. 1. Schematic illustration of the scattering problem of a PT-symmetric model considered in the present paper.

be represented by the infinite space and the corresponding measurements may be described by solving the scattering problem in an infinite space. This motivates us to study the scattering problem of a non-Hermitian system from the perspective of measuring the conductance of a PT-symmetric system. The non-Hermitian scattering problem for a PT-symmetric model has been discussed in different contexts [42–46].

We find here the following counterintuitive result: (i) when the non-Hermitian scattering potential is weak, the non-Hermitian signature is strong in that the transmission probability continuously exceeds unity and occasionally diverges; (ii) when the non-Hermitian scattering potential goes beyond a threshold, the Hermiticity is seemingly recovered in that the transmission probability shows a Fabry-Pérot-type peak structure with all the peaks being less than unity.

To contrast the present result with the standard behavior of PT-symmetric systems, let us briefly review the solution of a prototypical PT-symmetric model prescribed by the following two-site Hamiltonian:

$$H := \begin{pmatrix} i\gamma & t_{\mathrm{h}} \\ t_{\mathrm{h}} & -i\gamma \end{pmatrix}, \qquad (1)$$

where t_{h} represents the amplitude of hopping between the two sites, while $\pm i\gamma$ give a pair of two imaginary potentials compatible with PT symmetry. The spectrum of Eq. (1) is given by

$$E := \pm\sqrt{t_{\mathrm{h}}^2 - \gamma^2}; \qquad (2)$$

they are both real in the regime of weak non-Hermiticity $|\gamma| < |t_{\mathrm{h}}|$, which is often called the PT-unbroken phase, while they are both imaginary in the regime of strong non-Hermiticity $|\gamma| > |t_{\mathrm{h}}|$, which is referred to as the PT-broken phase. The Hamiltonian H in Eq. (1) commutes with the PT operator as in

$$(\hat{P}\hat{T})H(\hat{P}\hat{T})^{-1} = H, \qquad (3)$$

or $[H, \hat{P}\hat{T}] = 0$, where P is the parity operator,

$$\hat{P} := \begin{pmatrix} 0 & 1 \\ 1 & 0 \end{pmatrix}, \qquad (4)$$

and $\hat{T}$ is the time-reversal operator, which in the present case is the complex conjugation. Nonetheless, the eigenstates of H may not be the simultaneous eigenstates of PT because T is an antilinear operator [47]. They are indeed the simultaneous eigenstates in the PT-unbroken phase, but not in the PT-broken one; an eigenstate $|\psi_n\rangle$ is parallel to $\hat{P}\hat{T}|\psi\rangle$ in the former, while the two states are the respective eigenvectors of the imaginary eigenvalues $E = \pm i\sqrt{\gamma^2 - t_{\mathrm{h}}^2}$ in the latter.

The boundary between the two phases is marked with an exceptional point $|\gamma| = |t_{\mathrm{h}}|$, at which the two eigenvectors of Eq. (1) become parallel to each other and the corresponding eigenvalues coalesce [48]. Note that this is distinctive of non-Hermitian systems; all eigenvectors would be perpendicular to each other in Hermitian systems even when the eigenvalues are degenerate.

This example demonstrates that a non-Hermitian PT-symmetric system changes its nature drastically at the exceptional point $|\gamma| = |t_{\mathrm{h}}|$. To detect the physics of the exceptional point, however, one would have to connect the isolated PT-symmetric system to a Hermitian probe. This motivates us to analyze an open PT-symmetric system shown in Fig. 1, in which a non-Hermitian model is connected to Hermitian leads. As we stressed above, we make an observation here for the transmission probability that is quite opposite to the one for the system (1). The transmission probability exhibits strong signatures of non-Hermiticity in the weakly non-Hermitian regime, while it converges to a familiar Fabry-Pérot-type peak structure.

We first present in Sec. II a tutorial case of a single onsite non-Hermitian scatterer in an infinite tight-binding chain, in which we demonstrate that the transmission probability indicates the location of the exceptional point, a boundary between the PT-unbroken phase and the PT-broken phase. Using the results of the transmission and reflection coefficients for the single scatterer, we obtain in Sec. III A those for a PT-symmetric pair of scatterers in the framework of the Fabry-Pérot-type calculation. We confirm these results in a more universal framework in Sec. III B. We then describe in Sec. IV the peak structures of the transmission and reflection coefficients in terms of the Fabry-Pérot resonance and point-spectral complex eigenvalues of resonant states. We present in Sec. V the corresponding results for the continuum model with a pair of PT-symmetric δ potentials, before concluding in Sec. VI. We present a brief review in Appendix A for the point-spectral complex eigenvalues in open quantum systems, and details of the analytic calculations are presented in Appendix B.

II. TUTORIAL CASE OF THE SINGLE ON-SITE SCATTERER $i\gamma$: COLLIDING PEAKS AT THE EXCEPTIONAL POINT

One of our motivations here is to see in an infinite open quantum system the physics of the exceptional point typical in the two-site PT-symmetric model (1). It indeed manifests itself in the following simplest non-Hermitian scattering problem. We show its solutions for tutorial purposes; we also utilize them in Sec. III A when solving the scattering problem of the PT-symmetric scatterer by the Fabry-Pérot-type formulation.

Let us consider the following minimal but non-Hermitian scattering problem:

$$H := t_{\mathrm{h}} \sum_{x=-\infty}^{\infty} (|x+1\rangle\langle x| + |x\rangle\langle x+1|) + i\gamma|0\rangle\langle 0|, \qquad (5)$$

where t_{h} denotes the amplitude of the hopping element, whose sign we do not specify for the moment. The integer x

specifies a lattice site $x = 0, \pm 1, \pm 2, \ldots$; the lattice constant a is chosen to be unity. Our scattering potential is an isolated single on-site scatterer $i\gamma$ at $x = 0$, where γ is a real parameter with its sign not specified for the moment. On each side of the scattering potential at the origin, the wave function is presumed to have the form

$$\psi_x = \begin{cases} Ae^{ikx} + Be^{-ikx} & \text{for } x \leqslant 0, \\ Ce^{ikx} & \text{for } x \geqslant 0, \end{cases} \quad (6)$$

where ψ_x is short for $\langle x | \psi \rangle$ and $k > 0$. Then, the continuity of the wave function at $x = 0$ reinforces

$$\psi_0 = A + B = C. \quad (7)$$

Under the boundary condition (6), we solve the Schrödinger equation

$$H|\psi\rangle = E|\psi\rangle, \quad (8)$$

where

$$|\psi\rangle := (\ldots, \psi_{-1}, \psi_0, \psi_1, \ldots)^t. \quad (9)$$

Away from the scattering potential $x = 0$, the Schrödinger equation gives the dispersion relation

$$E(k) := 2t_{\mathrm{h}} \cos k. \quad (10)$$

At $x = 0$, on the other hand, it reads

$$t_{\mathrm{h}}(\psi_{-1} + \psi_1) + i\gamma\psi_0 = E(k)\psi_0. \quad (11)$$

Together with Eqs. (6), (7), and (10), Eq. (11) gives the transmission probability $T(k)$ of the incident wave in the form of $T(k) := |\mathcal{T}(k)|^2$, where the transmission coefficient $\mathcal{T}(k)$ is given by

$$\mathcal{T}(k) = \frac{C}{A} = \frac{2t_{\mathrm{h}} \sin k}{2t_{\mathrm{h}} \sin k + \gamma}. \quad (12)$$

Remarkably, the scattering amplitude $\mathcal{T}(k)$ diverges at

$$k = -\arcsin \frac{\gamma}{2t_{\mathrm{h}}}, \quad (13)$$

which can occur when $|\gamma| < 2|t_{\mathrm{h}}|$. The reflection probability is $R(k) := |\mathcal{R}(k)|^2$, where the reflection coefficient $\mathcal{R}(k)$ is given by

$$\mathcal{R}(k) := \frac{B}{A} = \frac{-\gamma}{2t_{\mathrm{h}} \sin k + \gamma}, \quad (14)$$

and hence it has the same peak structure. Physically, this divergence in the transmission and reflection coefficients can be regarded as an electronic analog of lasing [44,49], and it is due to a resonance pole incident on the real k axis (cf. the discussion below on discrete eigenvalues under the Siegert boundary condition). In Ref. [44], this phenomenon is referred to as *resonance state in continuum* (RIC), while in the literature a similar resonance structure has also been called a *spectral singularity* [50–56].

For the gain $\gamma > 0$, the divergence condition (13) is met with $k > 0$, which is a standard assumption in the scattering problem (6). This divergence realizes a situation of electronic analog of lasing. For a lossy potential $\gamma < 0$, on the other hand, the same condition is met with $k < 0$. In this case, the divergence realizes a situation of coherent perfect absorption [49,57,58].

Note that in normal crystals, the hopping amplitude is usually negative: $t_{\mathrm{h}} < 0$. However, if we prepare a specific type of crystal, either electronic or photonic, in which $t_{\mathrm{h}} > 0$, the role of gain and lossy potential is reversed. Under this consideration, we hereafter fix $\gamma > 0$ and $t_{\mathrm{h}} < 0$ for simplicity.

In Fig. 2, we plot the transmission probability $T(E)$ as a function of energy E in the two representative regimes: (a) $\gamma < 2|t_{\mathrm{h}}|$ and (b) $\gamma > 2|t_{\mathrm{h}}|$. In panel (a) [$\gamma = 1.9$ with $t_{\mathrm{h}} = -1$] the transmission probability $T(E)$ shows divergent peaks at the two values of E ($= E_1, E_2$) that satisfy Eq. (13). The existence of such divergent peaks in $T(E)$ in this relatively weak γ regime ($|\gamma| < 2|t_{\mathrm{h}}|$) is a strongly non-Hermitian behavior atypical in Hermitian systems. The two peaks at E_1 and E_2 get closer to one another as γ approaches $2|t_{\mathrm{h}}|$, they "collide" at $\gamma = 2|t_{\mathrm{h}}|$, and they transform into a broad peak after the collision, as shown in panel (b) [$\gamma = 2.1$ ($t_{\mathrm{h}} = -1$)]. This type of a broad peak of height $T(E) > 1$ in the strong γ regime ($\gamma > 2|t_{\mathrm{h}}|$) is still different from a Hermitian behavior, but it is less singular than the one in the weak γ regime.

This qualitative change of the behavior in $T(E)$ at $\gamma = 2|t_{\mathrm{h}}|$ is related to the fact that this point falls on an exceptional point in the parameter space. To clarify this, let us consider discrete eigenvalues, namely point spectra, of an open system under the Siegert boundary condition [59,60], that is, we set $A = 0$ in Eq. (6) so that there may be no incident wave. This boundary condition is known to produce all discrete eigenvalues of open quantum systems, including bound states and resonant states, which coincide with all the poles of the S-matrix in general and of the transmission probability in one dimension [61]; see Appendix A.

In the present case, the Siegert boundary condition signifies

$$\psi_{-1} = \psi_1 = \psi_0 e^{ik}. \quad (15)$$

Substituting this into Eq. (11), one can rewrite it as

$$(t_{\mathrm{h}}\beta^2 + i\gamma\beta - t_{\mathrm{h}})\psi_0 = 0, \quad (16)$$

where $\beta = e^{ik}$. To have a nontrivial solution $\psi_0 \neq 0$, we solve the quadratic equation

$$t_{\mathrm{h}}\beta^2 + i\gamma\beta - t_{\mathrm{h}} = 0, \quad (17)$$

finding the solutions $\beta_{\pm} = (-i\gamma \pm \sqrt{4t_{\mathrm{h}}^2 - \gamma^2})/(2t_{\mathrm{h}})$, which produce the two eigenvalues in the complex energy plane in the form

$$E_{\pm} = t_{\mathrm{h}}\left(\beta_{\pm} + \frac{1}{\beta_{\pm}}\right) = \pm\sqrt{4t_{\mathrm{h}}^2 - \gamma^2}. \quad (18)$$

Indeed, the divergence condition (13) is equivalent to Eq. (17). The transmission probability $T = |C/A|^2$ becomes infinite at its divergence implying $A \to 0$, while under the Siegert boundary condition, the condition $A = 0$ is preassigned.

Figure 2(c) shows how the two eigenvalues change in the complex energy plane as we vary the parameter $\gamma/|t_{\mathrm{h}}|$. When $\gamma < 2|t_{\mathrm{h}}|$, Eq. (17) has two solutions β_+ and β_- with their corresponding eigen-wave-number $k_{\pm} = -i \ln \beta_{\pm}$, which are both on the real axis. The eigenvalues $E_{\pm} = 2t_{\mathrm{h}} \cos k_{\pm}$ are also on the real axis. Correspondingly, the transmission probabilities $T(k)$ and $T(E)$ diverge at these values of k or E. When $\gamma > 2|t_{\mathrm{h}}|$, the two solutions $E_{\pm}$ become purely imaginary. Therefore, $T(E)$ no longer shows a divergence on the real
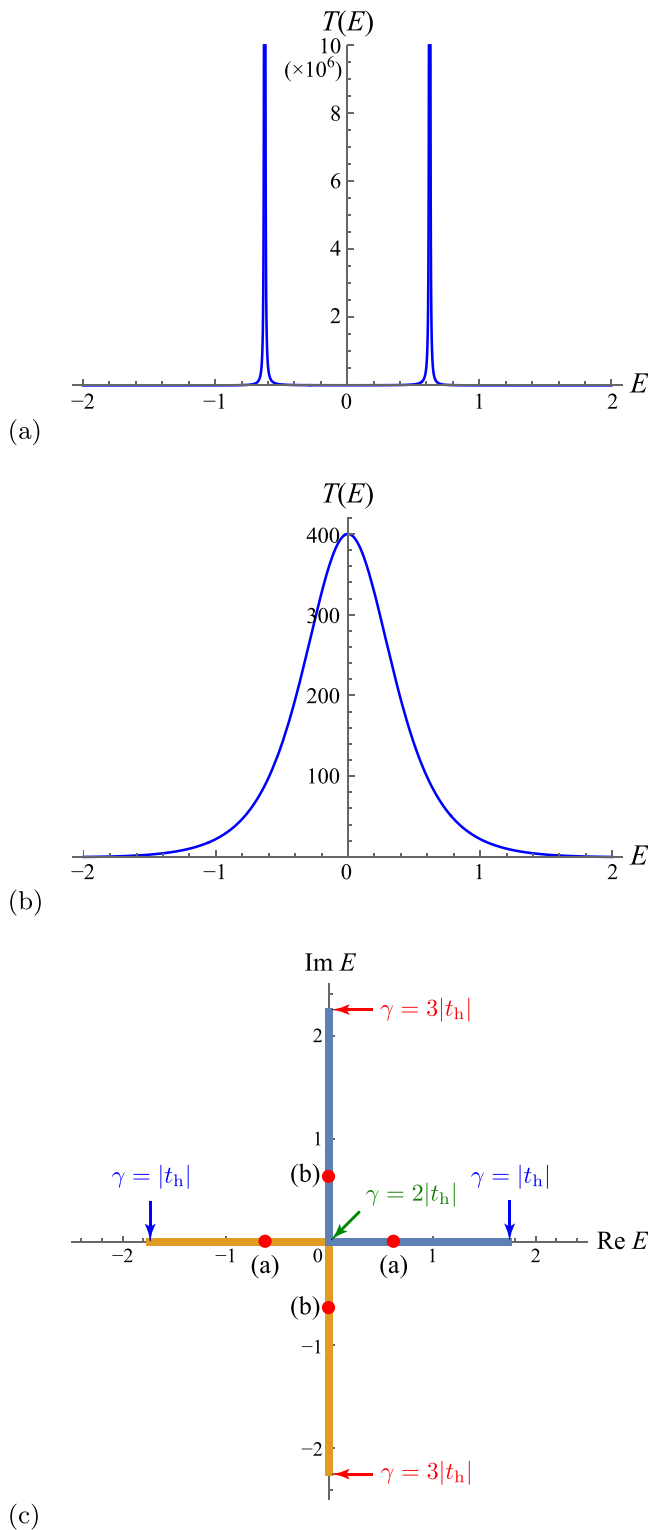
(a)

(b)

(c)

FIG. 2. Scattering peaks in the complex potential model (a) before and (b) after the collision of peaks at the exceptional point; specifically, (a) $\gamma = 1.9$ and (b) $\gamma = 2.1$ both with $t_h = -1$. (c) The change of the discrete eigenvalue (18) (thick lines) in the complex energy plane due to the variation of γ from $|t_h|$ to $3|t_h|$ with $t_h = -1$. The two complex eigenvalues collide at $E = 0$ in the case of the exceptional point $\gamma = 2|t_h|$. The dots on the real and imaginary axis, respectively, correspond to the cases of (a) and (b).

axis on which it is defined. The transmission probability $T(E)$ instead shows a typical Breit-Wigner peak at $E = 0$.

The condition $\gamma = 2|t_h|$ sets an exceptional point at which the two real eigenvalues collide and turn into a pair of two purely imaginary values, as we can see in Eq. (18). The collision occurs at $E = 0$ in the complex E plane. In the complex k plane, the eigenvalues are first on the real axis, they collide at $k = \pi/2$, and they split into a pair $k = \pi/2 \pm i\kappa$ with $\kappa > 0$.

Before and after the collision of eigenvalues at the exceptional point [cases (a) and (b) in Fig. 2(c), respectively], the nature of the eigenmodes is very different. When $\gamma < 2|t_h|$, i.e., when the transfer element $|t_h|$ to the neighboring sites is large enough, the probability amplitude emitted from the gain smoothly spreads out of the potential region, forming two outgoing plane waves, e^{ikx} and e^{-ikx}, which are indeed consistent with the Siegert boundary condition (A1). At the specific value of k determined by the values of γ and t_h as in Eq. (13), these two plane-wave solutions represent the nature of two poles on the real energy axis in case (a).

On the other hand, when γ exceeds $2|t_h|$, this smooth spread of the probability amplitude becomes no longer possible; the relatively small value of t_h does not allow the free spreading. Instead, for the eigenvalue $k = \pi/2 + i\kappa$, the probability amplitude starts to stay in the vicinity of the potential site, leading to an exponentially decaying wave function $e^{-\kappa|x|}$, i.e., a sort of pseudo-bound-state is formed. The formation of such a bound state (or a peculiar form of resonant state) is specific to non-Hermitian systems. For the eigenvalue $k = \pi/2 - i\kappa$, on the other hand, the probability amplitude spreads slowly, which corresponds to a resonant state with an exponentially increasing wave function of the form $e^{\kappa|x|}$; note that a resonant state in a Hermitian scattering problem also exhibits this type of a wave function. In Fig. 2(c), the two eigenvalues on the imaginary E axis [case (b)], one on the side of Im$E > 0$ and the other on the side of Im$E < 0$, respectively, represent these bound-state-like and resonant states. The two eigenvalues both contribute to the formation of a broad finite transmission peak.

In the scattering problem, we consider the transmission coefficient at real k and E, while the resonant poles in the large γ regime are *off* the real axis. As a result, a Breit-Wigner-type formula [62] for the transmission coefficient holds, leading to a finite, broadened transmission peak; the width of the peak is determined by the imaginary part of k or E [cf. Eq. (56)]. This is contrasting to the case of the small-γ regime in which the resonant poles are *on* the real axis, leading to a sharp divergent peak.

As the nature of eigenmodes evolves from plane-wave-like to resonant/bound-state-like behavior, the two eigenvalues on the real axis [case (a)] collide at the exceptional point $E = 0$ into the ones on the imaginary axis [case (b)]. In the present model (5), there exists a clear direct correspondence between this collision of the eigenvalues at the exceptional point and the drastic change of behavior of $T(E)$; at the exceptional point, a pair of sharp divergent peaks also collide and turn into a broad finite peak.

Let us finally comment on the unitarity of the S-matrix, i.e., on the behavior of the sum of the transmission and reflection

probabilities. Using Eqs. (12) and (14), we have

$$T(k) + R(k) = \frac{4t_h^2 \sin^2 k + \gamma^2}{4t_h^2 \sin^2 k + \gamma^2 + 4t_h \gamma \sin k}. \tag{19}$$

In the standard case of $t_h < 0$, the sign of the last term in the denominator depends on the sign of the parameter γ because $k > 0$. Therefore, $T(k) + R(k) > 1$ if $\gamma > 0$ and $T(k) + R(k) < 1$ if $\gamma < 0$. This is indeed consistent with the fact that the scattering potential is a source if $\gamma > 0$ and a sink if $\gamma < 0$. Anyway, the unitarity of the S-matrix is always broken: $T + R \neq 1$.

III. SCATTERING PROBLEM OF A PT-SYMMETRIC SCATTERER

Let us now come to the main point of the present paper and consider the scattering problem of a pair of on-site scatterers $i\gamma$ and $-i\gamma$, as is shown in Fig. 1. The model is specified by the Hamiltonian

$$H = t_h \sum_{x=-\infty}^{\infty} (|x+1\rangle\langle x| + |x\rangle\langle x+1|)$$
$$+ V_0|0\rangle\langle 0| + V_L|L\rangle\langle L|, \tag{20}$$

where V_0 and V_L are on-site scattering potentials, for which, unless otherwise specified, we consider the non-Hermitian PT-symmetric case: $V_0 = i\gamma$ and $V_L = -i\gamma$. (We mention other cases at the end of Sec. IV C.) We also consider the case $\gamma > 0$. The scattering region falls on $x \in [0, L]$. The case of $L = 2$ has been studied in Ref. [44]. We can confirm the PT-symmetry by reflecting the system with respect to the point $x = L/2$ and take the complex conjugation. The sign of t_h depends on the actual physical setups, as is Sec. II, but we take $t_h < 0$ except where indicated.

We will find the transmission and reflection probabilities in two ways. We first use a Fabry-Pérot-type formulation in Sec. III A. We then derive the same formulas by using a more universal formulation of solving the scattering problem in Sec. III B.

A. Fabry-Pérot formulas for the transmission and reflection probabilities

We first assume the incident and reflective waves on the left of the scattering region, and the transmissive wave on its right:

$$\psi_x = \begin{cases} Ae^{ikx} + Be^{-ikx} & \text{for } x \leqslant 0, \\ Ce^{ikx} & \text{for } x \geqslant L. \end{cases} \tag{21}$$

Our aim is to obtain the transmission and reflection coefficients, $\mathcal{T} := C/A$ and $\mathcal{R} := B/A$.

We try to find the transmissive wave from the left of the potential $+i\gamma$ to the right of the potential $-i\gamma$ as a superposition of the following: (i) The wave that transmits each of the two potentials; (ii) the wave that transmits the left potential, reflects at the right potential, reflects back at the left potential, and transmits the right potential; (iii) the wave that goes back and forth between the two potentials twice more; (iv) and so on; see Fig. 3. More specifically, for an incident wave of amplitude A at $x = 0$, we represent the transmissive wave
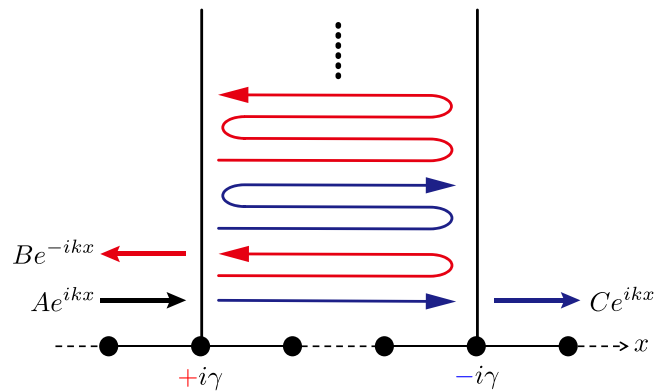

FIG. 3. The Fabry-Pérot-type calculation of the contributions to the transmissive wave (the blue lines) and to the reflective wave (the red lines).

$\psi_L := \langle L|\psi\rangle = Ce^{ikL}$ in terms of the following infinite series:

$$Ce^{ikL} = A\mathcal{T}_0 e^{ikL}\mathcal{T}_L + A\mathcal{T}_0 e^{ikL}\mathcal{R}_L e^{ikL}\tilde{\mathcal{R}}_0 e^{ikL}\mathcal{T}_L + \cdots$$
$$= \frac{A\mathcal{T}_0 \mathcal{T}_L e^{ikL}}{1 - \mathcal{R}_L \tilde{\mathcal{R}}_0 e^{2ikL}}, \tag{22}$$

where $\mathcal{T}_0$, $\mathcal{T}_L$, $\mathcal{R}_L$, and $\tilde{\mathcal{R}}_0$ are elements of the S-matrices for the potentials $\pm i\gamma$ at $x = 0$ and $x = L$; namely, the S-matrix for the potential $+i\gamma$ at $x = 0$ reads

$$S_0 = \begin{pmatrix} \mathcal{R}_0 & \tilde{\mathcal{T}}_0 \\ \mathcal{T}_0 & \tilde{\mathcal{R}}_0 \end{pmatrix}, \tag{23}$$

while that for the potential $-i\gamma$ at $x = L$ reads

$$S_L = \begin{pmatrix} \mathcal{R}_L & \tilde{\mathcal{T}}_L \\ \mathcal{T}_L & \tilde{\mathcal{R}}_L \end{pmatrix}. \tag{24}$$

We know from the results in Sec. II that

$$\mathcal{T}_0 = \frac{2t_h \sin k}{2t_h \sin k + \gamma}, \quad \mathcal{R}_0 = \frac{-\gamma}{2t_h \sin k + \gamma}. \tag{25}$$

Since the scattering problem for a single on-site scatterer is symmetric with respect to the potential, the coefficients due to the incident wave from the right should be equal to the equivalent coefficients from the left: $\tilde{\mathcal{T}}_0 = \mathcal{T}_0$ and $\tilde{\mathcal{R}}_0 = \mathcal{R}_0$.

For $\mathcal{T}_L$ and $\mathcal{R}_L$, we only need to flip the sign of the parameter γ because the potential there is $-i\gamma$ instead of $+i\gamma$. Therefore, we have

$$\mathcal{T}_L = \frac{2t_h \sin k}{2t_h \sin k - \gamma}, \quad \mathcal{R}_L = \frac{\gamma}{2t_h \sin k - \gamma}. \tag{26}$$

According to the same argument for S_0, we should have $\tilde{\mathcal{T}}_L = \mathcal{T}_L$ and $\tilde{\mathcal{R}}_L = \mathcal{R}_L$.

Substituting the expressions in Eqs. (25) and (26) into Eq. (22), we arrive at

$$\mathcal{T}(k) = \frac{C}{A} = \frac{4t_h^2 \sin^2 k}{4t_h^2 \sin^2 k + \gamma^2(e^{2ikL} - 1)}. \tag{27}$$

We will find the same expression from the standard way of solving the scattering problem in Sec. III B.

We can derive the reflection coefficient $\mathcal{R}$ in the same way. In parallel with Eq. (22), we find the amplitude B for the

reflective wave in the form

$$
\begin{aligned}
B &= A\mathcal{R}_0 + A\mathcal{T}_0 e^{ikL}\mathcal{R}_L e^{ikL}\tilde{\mathcal{T}}_0 \\
&\quad + A\mathcal{T}_0 e^{ikL}\mathcal{R}_L e^{ikL}\tilde{\mathcal{R}}_0 e^{ikL}\mathcal{R}_L e^{ikL}\tilde{\mathcal{T}}_0 + \cdots \\
&= A\mathcal{R}_0 + \frac{A\mathcal{T}_0\mathcal{R}_L\tilde{\mathcal{T}}_0 e^{2ikL}}{1 - \mathcal{R}_L\tilde{\mathcal{R}}_0 e^{2ikL}}.
\end{aligned}
\tag{28}
$$

After straightforward algebra, we find

$$
\begin{aligned}
\mathcal{R}(k) = \frac{B}{A} &= \mathcal{R}_0 + \mathcal{R}_L e^{2ikL}\mathcal{T}(k) \\
&= \frac{\gamma(2t_h \sin k - \gamma)(e^{2ikL} - 1)}{4t_h^2 \sin^2 k + \gamma^2(e^{2ikL} - 1)}.
\end{aligned}
\tag{29}
$$

We will also find the same expression in Sec. III B.

We can similarly find the transmission and reflection coefficients $\tilde{\mathcal{T}}$ and $\tilde{\mathcal{R}}$ due to the incident wave from the right. These coefficients have the expressions in which the sign of the parameter γ is flipped in $\mathcal{T}$ and $\mathcal{R}$ because the first potential that the incident wave from the right meets is that of $-i\gamma$ instead of $+i\gamma$. Since $\mathcal{T}(k)$ is an even function of γ, we easily find $\tilde{\mathcal{T}}(k) = \mathcal{T}(k)$, but $|\mathcal{R}| \neq |\tilde{\mathcal{R}}|$ in contrast; in other words, our transmission coefficients are reciprocal, while the reflection coefficients are nonreciprocal. This type of non-reciprocal transport is possible in a non-Hermitian system with parity broken but transposition unbroken (for details, see Sec. 6.1 of Ref. [1]).

B. More universal way of solving the problem

We can solve the potential-scattering problem in the following standard formulation, too. We again assume the form (21). The Schrödinger equations at the sites $x = 0, 1, 2, \ldots, L$ thereby read

$$
\begin{aligned}
t_h(\psi_{-1} + \psi_1) + i\gamma\psi_0 &= E\psi_0, \\
t_h(\psi_0 + \psi_2) &= E\psi_1, \\
&\cdots \\
t_h(\psi_{L-2} + \psi_L) &= E\psi_{L-1}, \\
t_h(\psi_{L-1} + \psi_{L+1}) - i\gamma\psi_L &= E\psi_L.
\end{aligned}
\tag{30}
$$

The remaining equations for $x < 0$ and $x > L$ simply give the dispersion relation (10).

We can cast the open set of equations (30) into a closed matrix equation in the following way. In the list of equations (30), we express the wave-function amplitudes one step outside of the scattering region, namely ψ_{-1} and ψ_{L+1}, in terms of the amplitudes inside the scattering region $x \in [0, L]$. Utilizing Eq. (21), we have

$$
\begin{aligned}
\psi_{-1} &= Ae^{-ik} + Be^{ik} = Ae^{-ik} + (\psi_0 - A)e^{ik} \\
&= -2iA\sin k + e^{ik}\psi_0
\end{aligned}
\tag{31}
$$

and

$$
\psi_{L+1} = Ce^{ik(L+1)} = e^{ik}\psi_L
\tag{32}
$$

because $\psi_0 = A + B$ and $\psi_L = Ce^{ikL}$. Inserting Eqs. (31) and (32) into the first and last equations of Eqs. (30), we arrive at

the closed $(L + 1)$-dimensional matrix equation

$$
M_L \begin{pmatrix} \psi_0 \\ \psi_1 \\ \vdots \\ \psi_{L-1} \\ \psi_L \end{pmatrix} = \begin{pmatrix} \tilde{A} \\ 0 \\ \vdots \\ 0 \\ 0 \end{pmatrix},
\tag{33}
$$

where

$$
\tilde{A} = 2iAt_h \sin k,
\tag{34}
$$

and an $(L + 1) \times (L + 1)$ matrix

$$
M_L = H_L - E(k)I_{L+1} = H_L - t_h(e^{ik} + e^{-ik})I_{L+1}
\tag{35}
$$

with H_L denoting an effective Hamiltonian matrix

$$
H_L = \begin{pmatrix}
i\gamma + t_h e^{ik} & t_h & & & \\
t_h & & t_h & & \\
& t_h & & \ddots & \\
& & \ddots & & t_h \\
& & & t_h & -i\gamma + t_h e^{ik}
\end{pmatrix}
\tag{36}
$$

and I_{L+1} denoting the $(L + 1)$-dimensional identity matrix.

Using Eqs. (33)–(36), we can derive the transmission and reflection coefficients as follows. Equation (33) implies

$$
\psi_0 = (M_L^{-1})_{1,1}\tilde{A},
\tag{37}
$$

$$
\psi_L = (M_L^{-1})_{L+1,1}\tilde{A},
\tag{38}
$$

which read

$$
1 + \frac{B}{A} = 2it_h(M_L^{-1})_{1,1}\sin k,
\tag{39}
$$

$$
\frac{C}{A}e^{ikL} = 2it_h(M_L^{-1})_{L+1,1}\sin k.
\tag{40}
$$

We can thus obtain $\mathcal{T} = C/A$ and $\mathcal{R} = B/A$ by finding the two elements of the inverted matrix M_L^{-1}.

The inversion of the matrix M_L involves computation of matrix determinants by means of recursion equations. The algebra given in Appendix B produces exactly the same expressions as Eqs. (27) and (29). We can thus validate the calculation based on the Fabry-Pérot-type formulation.

IV. CONTRASTING BEHAVIOR OF $T(k)$ AND $R(k)$ IN THE WEAK AND STRONG γ REGIMES

A. Transmission and reflection probabilities

Figure 4 shows the transmission probability $T(k) = |C/A|^2$ of the system with $L = 7$, which exemplifies the generic case of odd L. The behavior is quite different between a region of weak non-Hermiticity, namely $\gamma < 2|t_h|$, and a region of strong non-Hermiticity, $\gamma > 2|t_h|$. Note that the critical value $\gamma = 2|t_h|$ corresponds to the exceptional point in the problem of the single on-site scatterer that we considered in Sec. II.

In the region of weak non-Hermiticity, $\gamma < 2|t_h|$, the transmission probability $T(k)$ (represented by bluish curves) shows a peak higher than unity. Such behavior is common in a non-Hermitian scattering problem; in the most prototypical case of a single isolated on-site scatterer $i\gamma$ analyzed in Sec. II, the transmission probability $T(k)$ can not only exceed unity
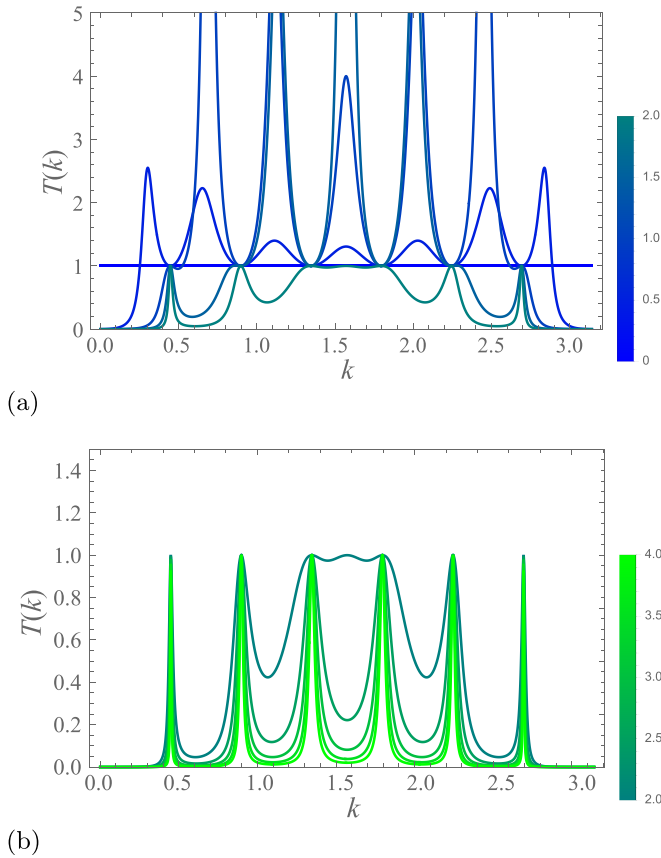
(a)

(b)

FIG. 4. Variation of the transmission probability $T(k)$ for $L = 7$; (a) in the weak regime, $\gamma < 2|t_{\rm h}|$ ($\gamma/|t_{\rm h}| = 0, 0.5, 1, 1.5, 2$), and (b) in the strong regime, $\gamma > 2|t_{\rm h}|$ ($\gamma/|t_{\rm h}| = 2, 2.5, 3, 3.5, 4$). The color bars show the value of $\gamma/|t_{\rm h}|$.

(a)

(b)

FIG. 5. Variation of the reflection probabilities for $L = 7$ at $\gamma/|t_{\rm h}| = 0.5, 1, 1.5, \ldots, 3.5, 4$; the color bar shows the value of $\gamma/|t_{\rm h}|$. (a) $R(k)$ for the incident wave from the left and (b) $\tilde{R}(k)$ for the incident wave from the right.

but can diverge for some values of k at the point that satisfies Eq. (13). In the present PT-symmetric case, the transmission peaks are not generally divergent but exceed unity, particularly in the region of weak non-Hermiticity. The divergence occurs for specific values of γ given in Eq. (47) at the values of k given in Eq. (48).

In the region $\gamma > 2|t_{\rm h}|$, on the other hand, the situation is superficially Hermitian in contrast. The transmission probability T (represented by greenish curves) still shows peaks, but their height is bounded by unity, $T(k) \leqslant 1$, which is common in the Hermitian case. These peaks are consistent with the conventional Fabry-Pérot-type resonances at the wave numbers

$$ k = \frac{n\pi}{L}, \qquad (41) $$

where $n = 1, 2, \ldots, L - 1$. In Sec. IV B, we describe these results in terms of the analytical formula of the transmission probability.

The behavior of the reflection probability $R(k)$, on the other hand, is different from the one common in the Hermitian Fabry-Pérot case; in Fig. 5, $R(k)$ exhibits dips at the wave numbers given in Eq. (41), which itself is consistent with the Fabry-Pérot-type resonance, but its magnitude elsewhere breaks the unitarity of the S-matrix,

$$ T + R = |\mathcal{T}|^2 + |\mathcal{R}|^2 \neq 1, \qquad (42) $$
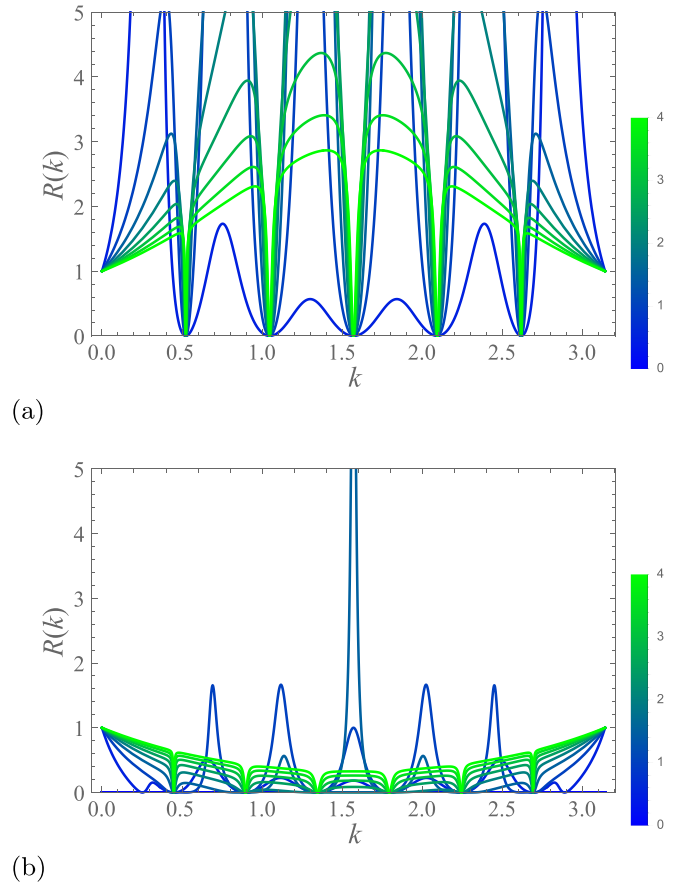
even in the superficially Hermitian regime $\gamma > 2|t_{\rm h}|$. The reflection probability due to the incident wave from the left exceeds unity except for the dips, while that due to the incident wave from the right is suppressed to less than unity. We present in Sec. IV D approximate functions of these profiles.

B. Understanding the peak structure of the transmission probability

We analyze here the drastic change of $T(k)$ at $\gamma = 2|t_{\rm h}|$ that we found in Fig. 4, from the point of view of the analytic formula (27) for the transmission coefficient. Let us first note that Eq. (27) yields the transmission probability $T(k) := |\mathcal{T}(k)|^2$ in the form

$$ T(k) = \frac{4t_{\rm h}^4 \sin^4 k}{4t_{\rm h}^4 \sin^4 k + \gamma^2 (\gamma^2 - 4t_{\rm h}^2 \sin^2 k) \sin^2 kL}, \qquad (43) $$

which is greater than unity, $T(k) > 1$, for $\gamma < 2|t_{\rm h}|$ in the following range of k:

$$ \arcsin \frac{\gamma}{2|t_{\rm h}|} < k < \pi - \arcsin \frac{\gamma}{2|t_{\rm h}|} \qquad (44) $$

so that the factor $(\gamma^2 - 4t_{\rm h}^2 \sin^2 k)$ may be positive. In the Fabry-Pérot regime $\gamma > 2|t_{\rm h}|$, on the other hand, it is always

less than unity:

$$T(k) < 1 \quad \text{for all } k \text{ when } \gamma > 2|t_{\mathrm{h}}|. \tag{45}$$

For $T(k)$ to be divergent, the denominator of Eq. (27) must vanish. Since the first term $4t_{\mathrm{h}}^2 \sin^2 k$ of the denominator is real and positive except at $k = 0$ and $k = \pi$, a divergent peak can appear for a generic value of k only when the complex factor e^{2ikL} happens to be real; in other words,

$$e^{2ikL} = \pm 1. \tag{46}$$

In the cases of $e^{2ikL} = 1$, peaks emerge, but they do not diverge because the second term of the denominator of Eq. (27) vanishes, and one trivially finds $\mathcal{T}(k) = 1$. This indeed corresponds to the spuriously Hermitian Fabry-Pérot peaks that we observe in the regime of $\gamma > 2|t_{\mathrm{h}}|$ [Fig. 4(b)]; indeed, $e^{2ikL} = 1$ is the Fabry-Pérot resonance condition. When $\gamma > 2|t_{\mathrm{h}}|$, we have the perfect transmission $T(k) = 1$ at each resonance point while $T(k) < 1$ off resonance because the second term dominates the denominator in Eq. (27) if $\gamma > 2|t_{\mathrm{h}}|$ and $e^{2ikL} \neq 1$.

Hereafter throughout the present section, we discuss the cases of $e^{2ikL} = -1$. In such cases, the denominator of Eq. (27) vanishes if

$$\gamma = \sqrt{2}|t_{\mathrm{h}}| \sin k. \tag{47}$$

This corresponds to the divergent peaks of $T(k)$ in the regime of $\gamma < 2|t_{\mathrm{h}}|$ [Fig. 4(a)]. To be more explicit, $e^{2ikL} = -1$ is satisfied at the values of k such that

$$k = k_n := \frac{(2n-1)\pi}{2L}, \tag{48}$$

where $n = 1, 2, \ldots, L$. The transmission probability $T(k)$ is divergent at $k = k_n$ when we tune the value of γ close to $\gamma_n := \sqrt{2}|t_{\mathrm{h}}| \sin k_n$, which is possible only when $\gamma \leqslant \sqrt{2}|t_{\mathrm{h}}| < 2|t_{\mathrm{h}}|$. The integer n that is responsible for the divergence changes as we vary γ. When we turn on γ, the first pair of peaks develop at $k = k_1$ and $k = k_L$, and diverge when we tune γ up to γ_1. As we increase γ from γ_1 toward γ_2, the first pair of peaks subside and the second pair of peaks start to grow at k_2 and k_{L-1}, which diverge when γ reaches γ_2. As we further increase γ, successive peaks appear at $k = k_3, \ldots$ on the side of $k < \pi/2$ and at $k = k_{L-2}, \ldots$ on the side of $k > \pi/2$. The divergent peaks thus moves toward $k = \pi/2$ from both sides [63].

When γ goes to $\sqrt{2}|t_{\mathrm{h}}|$ from below, what happens depends on the parity of L. If L is odd with $L = 2l - 1$ as in Fig. 4(a), the last divergent peak appears at the midpoint $k = k_l = \pi/2$ because it is contained in the set (48). At this point, Eq. (27) reduces to

$$\mathcal{T}(\pi/2) = \frac{2t_{\mathrm{h}}^2}{2t_{\mathrm{h}}^2 - \gamma^2}, \tag{49}$$

which diverges at $\gamma = \sqrt{2}|t_{\mathrm{h}}|$. Beyond this value of γ, the transmission probability at the midpoint subsides, and eventually lowers the unity when $\gamma > 2|t_{\mathrm{h}}|$ [Fig. 4(b)]. Since the peak at $k = \pi/2$ is the last divergent one as we increase γ, other peaks decay at even smaller values of γ, and hence no peak exceeds unity beyond $\gamma > 2|t_{\mathrm{h}}|$. This explains why the transmission probability $T(k)$ becomes superficially Hermitian in the regime of $\gamma > 2|t_{\mathrm{h}}|$. It may be worthwhile to
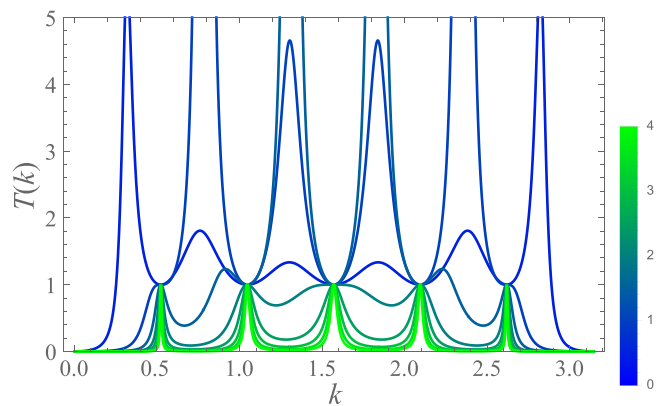

FIG. 6. Variation of the transmission probability $T(k)$ for $L = 6$ at $\gamma/|t_{\mathrm{h}}| = 0.5, 1, 1.5, \ldots, 3.5, 4$. The color bar shows the value of $\gamma/|t_{\mathrm{h}}|$. The bluish curves correspond to the weak regime, $\gamma < 2|t_{\mathrm{h}}|$, while the greenish ones correspond to the strong regime, $\gamma > 2|t_{\mathrm{h}}|$.

mention that $T(\pi/2)$ turns from a maximum to a minimum at $\gamma = 2|t_{\mathrm{h}}|$; see Figs. 4(a) and 4(b).

If L is even with $L = 2l$ as in Fig. 6, on the other hand, the last divergence occurs not at $k = \pi/2$ but at k_l and k_{l+1}, i.e., at

$$k = \frac{\pi}{2} \pm \frac{\pi}{2L} \tag{50}$$

at the same time. At these values of k, Eq. (27) reduces to

$$\mathcal{T}(k) = \frac{t_{\mathrm{h}}^2 [1 + \cos(\pi/L)]}{t_{\mathrm{h}}^2 [1 + \cos(\pi/L)] - \gamma^2}. \tag{51}$$

Therefore, the divergence of the last peaks at $k = k_l$ and $k = k_{l+1}$ occurs when we increase γ up to

$$\gamma = |t_{\mathrm{h}}| \sqrt{1 + \cos \frac{\pi}{L}} < \sqrt{2}|t_{\mathrm{h}}|. \tag{52}$$

When we further increase so that

$$\gamma > \sqrt{2}|t_{\mathrm{h}}| \sqrt{1 + \cos \frac{\pi}{L}} > \sqrt{2}|t_{\mathrm{h}}|, \tag{53}$$

Eq. (51) gives $T(k_l) = T(k_{l+1}) \leqslant 1$, i.e., a superficially Hermitian result. Meanwhile, $T(\pi/2)$ for even L is given under the condition $e^{2ikL} = 1$, and hence it turns from a minimum between the two peaks at k_l and k_{l+1} for $\gamma < 2|t_{\mathrm{h}}|$ into a maximum of the Fabry-Pérot-type for $\gamma > 2|t_{\mathrm{h}}|$ [63].

C. Discrete eigenvalues under the Siegert boundary condition

We can also understand the peak structure of the transmission probability from the locations of discrete eigenvalues. The discrete eigenvalues are given by the poles of the S-matrix, and hence in the present case the zeros of the denominator of $\mathcal{T}(k)$ and $\mathcal{R}(k)$ in Eqs. (27) and (29) [64]:

$$4t_{\mathrm{h}}^2 \sin^2 k_n + \gamma^2 (e^{2ik_n L} - 1) = 0. \tag{54}$$

In the present case, there are $2L$ pieces of generally complex solutions $\{k_n\}$, except at exceptional points, where two solutions coalesce; see Appendix A for a review. This implies that, except at the exceptional points, we may be able to break
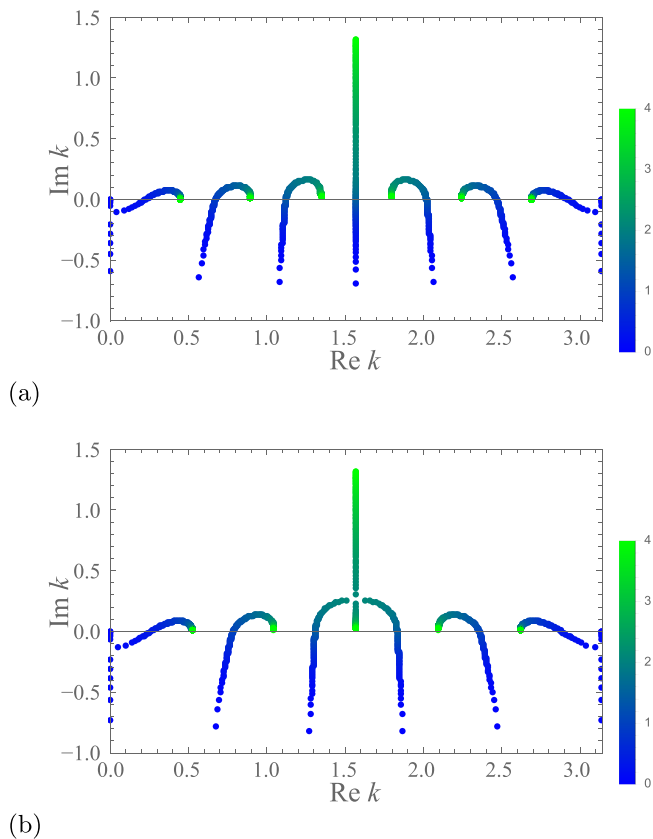
(a)

(b)

FIG. 7. Trajectories of discrete eigenvalues in the complex k plane. Cases of (a) $L = 7$ and (b) $L = 6$. The color bars show the value of $\gamma / |t_\mathrm{h}|$.

down $\mathcal{T}(k)$ into the form of the Laurent expansion:

$$\mathcal{T}(k) = \sum_{n=1}^{2L-2} \frac{c_n}{k - k_n} + f(k), \tag{55}$$

where $\{c_n\}$ are generally complex constants and $f(k)$ is a regular function with the standard Taylor expansion. Therefore, the most singular contributions to the transmission probability may be made of the Breit-Wigner-type ones [62]:

$$T(k) = |\mathcal{T}(k)|^2 \simeq \sum_{n=1}^{2L-2} \frac{|c_n|^2}{|k - k_n|^2}$$

$$= \sum_{n=1}^{2L-2} \frac{|c_n|^2}{\left(k - k_n^\mathrm{r}\right)^2 + k_n^\mathrm{i}{}^2}; \tag{56}$$

that is, a Lorentzian peak with its center at $k = k_n^\mathrm{r}$ and its half-width at half-maximum k_n^i. Indeed, this is what we see in Figs. 4 and 6.

Figure 7 shows the trajectories of the discrete eigenvalues in the complex k plane on the side of Re$k > 0$ for $L = 7$ and 6 [63]. (There are $2L$ pieces of eigenvalues, but only half of them are on this side of the k plane; the remaining half are on the side of Re$k < 0$ and are irrelevant to the present argument.)

Upon increasing the parameter γ, the eigenvalues leave trajectories that cross the real axis, which is responsible for the diverging peaks in the regime of weak non-Hermiticity,

$\gamma < 2|t_\mathrm{h}|$. When an eigenvalue is located on the real axis, we have $k^\mathrm{i} = 0$ in the Lorentzian (56), and hence the peak may diverge (except when the cancellation occurs with the numerator). The two eigenvalues on the far right and the far left first cross the real axis, and thereby generate the first two diverging peaks. The two neighboring eigenvalues next cross the real axis, generating the next two peaks. The third pair of eigenvalues generate the third pair of peaks, and so on. For odd values of L, in particular, the one in the middle generates the last divergence when it crosses the point $k = \pi/2$. These all happen in the weak non-Hermiticity regime.

We stress here that in Hermitian systems, the discrete eigenvalues are prohibited in the first quadrant [64]. In this sense, the divergence due to the eigenvalues crossing the real axis onto the first quadrant is a distinctively non-Hermitian phenomenon.

In the strong non-Hermiticity regime, $\gamma > 2|t_\mathrm{h}|$, the eigenvalues except for the one in the middle approach the points specified in Eq. (41), and they generate the Fabry-Pérot-type peaks there. In the case of $L = 7$, for example, there are six such peaks, that is, one less than the diverging peaks in the weak non-Hermiticity regime, because the eigenvalue with $k^\mathrm{r} = \pi/2$ keeps climbing up the complex k plane and does not contribute to the Fabry-Pérot peaks. In the case of $L = 6$, two eigenvalues closest to the point $k^\mathrm{r} = \pi/2$ eventually collide on the line $k = \pi/2$ forming an exceptional point, and one climbs up this line in the complex k plane, but the other comes back to the real axis, again making peaks one less than the diverging peaks in the weak non-Hermiticity regime. The eigenvalues come to the real axis only in the limit of $\gamma \to \infty$, which is, however, a trivial limit with $T \equiv 0$ and $R \equiv 1$ with the exception of $T = 1$ and $R = 0$ at the points (41). The Fabry-Pérot peaks do not diverge because Eq. (54) reduces to the Fabry-Pérot condition $e^{2ik_n L} = 1$ in the limit $\gamma \to \infty$, where the remaining first term in Eq. (54) cancels the numerator of Eq. (27), always giving a perfect transmission $\mathcal{T}(k) = 1$.

The exceptional point on the line $k = \pi/2$ appears only for even L. The change of the behavior of $T(k)$ at $\gamma = 2|t_\mathrm{h}|$ being the borderline is not directly related to the appearance of this exceptional point. Unlike the one in Eq. (2), this exceptional point located away from the real axis is not related to the breaking of PT symmetry either.

In the model (5) discussed in Sec. II, the region of weak non-Hermiticity $\gamma < 2|t_\mathrm{h}|$ falls on a superficially Hermitian region with two real eigenvalues, while that of strong non-Hermiticity $\gamma > 2|t_\mathrm{h}|$ with two imaginary eigenvalues is considered to be a truly non-Hermitian region. The roles of the two regimes seem to be consistent with the intuition that we have from the 2×2 model (1) in the Introduction. In our open PT-symmetric system (20), in contrast, real eigenvalues appear only occasionally in the regime $\gamma < 2|t_\mathrm{h}|$, and the most eigenvalues approach the real axis again in the limit of extremely strong non-Hermiticity.

The existence of the non-Hermitian Fabry-Pérot region is specific to the PT-symmetric choice of V_0 and V_L, i.e., $V_0 = i\gamma$ and $V_L = -i\gamma$. In a non-Hermitian but non-PT-symmetric choice of V_0 and V_L, e.g., $V_0 = V_L = i\gamma$ or $V_0 = V_L = -i\gamma$, Fabry-Pérot peaks such as the ones in the PT-symmetric case do not appear. In this sense the non-Hermitian

Fabry-Pérot region is protected by the PT-symmetry. In the case of real (Hermitian) scattering potentials, e.g., $V_0 = V_L = \gamma$ or $V_0 = -V_L = \gamma$, the Fabry-Pérot peak structure appears for an arbitrary finite γ, while unlike in the PT-symmetric case the discrete eigenvalues approach the real k axis from below in the limit of large γ. In the PT-symmetric case, the discrete eigenvalues approach the real k axis from above; see Fig. 7.

D. The reflection probability and the unitarity of the *S*-matrix

Let us turn our attention to the reflection probability and analyze its peak structure based on the analytic formula (29). Since the denominator is the same as that of $\mathcal{T}(k)$ in Eq. (27), the divergent behavior is common in the regime $\gamma < 2|t_h|$. The drastic difference is noticeable in the Fabry-Pérot region $\gamma > 2|t_h|$. The reflection probability $R(k)$ shows dips at k given in Eq. (41), corresponding to the Fabry-Pérot peaks in $T(k)$; compare Figs. 4(b) and 5(a). In between the dips, however, $R(k)$ remains greater than the unity, which does not seem Hermitian even in the Fabry-Pérot region $\gamma > 2|t_h|$.

We can understand this in the following way. Equation (29) yields the reflection probability $R(k) := |\mathcal{R}(k)|^2$ in the form

$$R(k) = \frac{\gamma^2(\gamma - 2t_h \sin k)^2 \sin^2 kL}{4t_h^4 \sin^4 k + \gamma^2(\gamma^2 - 4t_h^2 \sin^2 k) \sin^2 kL}. \quad (57)$$

Comparing Eqs. (43) and (57), we find

$$R(k) = \alpha(\gamma, k)[1 - T(k)], \quad (58)$$

where

$$\alpha(\gamma, k) := \frac{\gamma - 2t_h \sin k}{\gamma + 2t_h \sin k}. \quad (59)$$

Therefore, $R(k)$ is related to $1 - T(k)$, but it is modulated as in Eq. (58) by the function $\alpha(\gamma, k)$. Since $t_h < 0$ and $k > 0$, we have $\alpha(\gamma, k) > 1$ in the Fabry-Pérot region, $\gamma > 2|t_h|$, which we can confirm in Fig. 5(a).

Figure 5(b), on the other hand, shows the reflection probability $\tilde{R}(k)$ due to the incident wave from the right. This reflection probability shows dips at k given in Eq. (41) too, but in between the dips, $\tilde{R}(k)$ is suppressed to values less than unity.

This is understand in the following way, too. As we stated at the end of Sec. III A, we obtain the reflection probability $\tilde{R}(k)$ by flipping the sign of γ from $R(k)$:

$$\tilde{R}(k) = \frac{\gamma^2(-\gamma - 2t_h \sin k)^2 \sin^2 kL}{4t_h^4 \sin^4 k + \gamma^2(\gamma^2 - 4t_h^2 \sin^2 k) \sin^2 kL}. \quad (60)$$

Meanwhile, we have $\tilde{T}(k) = T(k)$. We therefore arrive at

$$\tilde{R}(k) = \frac{1}{\alpha(\gamma, k)}[1 - \tilde{T}(k)]. \quad (61)$$

Therefore, $\tilde{R}(k)$ is related to $1 - \tilde{T}(k)$, but it is modulated by the function $1/\alpha(\gamma, k)$, which is less than unity in the Fabry-Pérot region, $\gamma > 2|t_h|$. This is what we see in Fig. 5(b).

Let us finally analyze the sum of the transmission and reflection probabilities. We obtain

$$T(k) + R(k) - 1$$
$$= \frac{-4t_h\gamma^2 \sin k \sin^2 kL(\gamma - 2t_h \sin k)}{4t_h^4 \sin^4 k + \gamma^2(\gamma^2 - 4t_h^2 \sin^2 k) \sin^2 kL}. \quad (62)$$

The denominator is non-negative because it is the square modulus of the common denominator of Eqs. (27) and (29). The numerator is always positive because we assume $t_h < 0$, $\gamma > 0$, and $k > 0$. We thereby conclude that $T(k) + R(k) > 1$ always stands for the incident wave from the left. For the incident wave from the right, Eq. (62) is changed to

$$\tilde{T}(k) + \tilde{R}(k) - 1$$
$$= \frac{-4t_h\gamma^2 \sin k \sin^2 kL(-\gamma - 2t_h \sin k)}{4t_h^4 \sin^4 k + \gamma^2(\gamma^2 - 4t_h^2 \sin^2 k) \sin^2 kL}. \quad (63)$$

We have $\tilde{T}(k) + \tilde{R}(k) < 1$ in the Fabry-Pérot regime because $(-\gamma - 2t_h \sin k) \leqslant (-\gamma + 2|t_h|) < 0$ when we assume $\gamma > 0$, $t_h < 0$, and $k > 0$. Recall that the transmission is symmetric with respect to the direction of the incident wave, but the reflection is not.

The difference between the two inequalities (62) and (63) is consistent with the intuition that the potential that the incident wave first meets makes larger contributions to the Fabry-Pérot superposition (22): since the incident wave from the left meets the source $+i\gamma$ first, the flux is enhanced; on the other hand, since the incident wave from the right meets the sink $-i\gamma$ first, the flux is suppressed.

V. SCATTERING PROBLEM OF THE CONTINUUM MODEL

We finally describe what happens for the continuum model. Let us start with the tight-binding model, and consider its continuum limit. We first recover the lattice constant a, and we take the continuum limit in which we set $a \to 0$ and $L \to \infty$, keeping $\tilde{L} = La$ finite. In this process, we replace the on-site scattering potential $\pm i\gamma$ with $\pm i\gamma a$ so that they may converge to δ-function scatterers $V(x) = i\gamma\delta(x) - i\gamma\delta(x - \tilde{L})$ in the continuum limit. To reproduce the conventional kinetic term, we also make the following replacement: $-t_h a^2 = \hbar^2/(2m)$. Then, Eq. (27) reduces to

$$\mathcal{T}(k) = \frac{4k^2}{4k^2 + \tilde{\gamma}^2(e^{2ik\tilde{L}} - 1)}, \quad (64)$$

where we have introduced

$$\tilde{\gamma} = \frac{\gamma}{|t_h|} = \frac{2m}{\hbar^2}\gamma. \quad (65)$$

The same applies for Eq. (29), producing

$$\mathcal{R}(k) = \frac{-\tilde{\gamma}(2k + \tilde{\gamma})(e^{2ik\tilde{L}} - 1)}{4k^2 + \tilde{\gamma}^2(e^{2ik\tilde{L}} - 1)}. \quad (66)$$

The discrete eigenvalues are found from the zeros of the denominator:

$$4k^2 + \tilde{\gamma}^2(e^{2ik\tilde{L}} - 1) = 0. \quad (67)$$

We can of course find the same expressions by solving the the Schrödinger equation $H\psi(x) = E\psi(x)$ with the Hamiltonian,

$$H = -\frac{\hbar^2}{2m}\frac{d^2}{dx^2} + i\gamma\delta(x) - i\gamma\delta(x - \tilde{L}). \quad (68)$$

Figures 8(a) and 8(b) show, respectively, the transmission and reflection probabilities in the continuum limit, in which $\tilde{L}$ is chosen as $\tilde{L} = 3$ so that the separation of the Fabry-Pérot
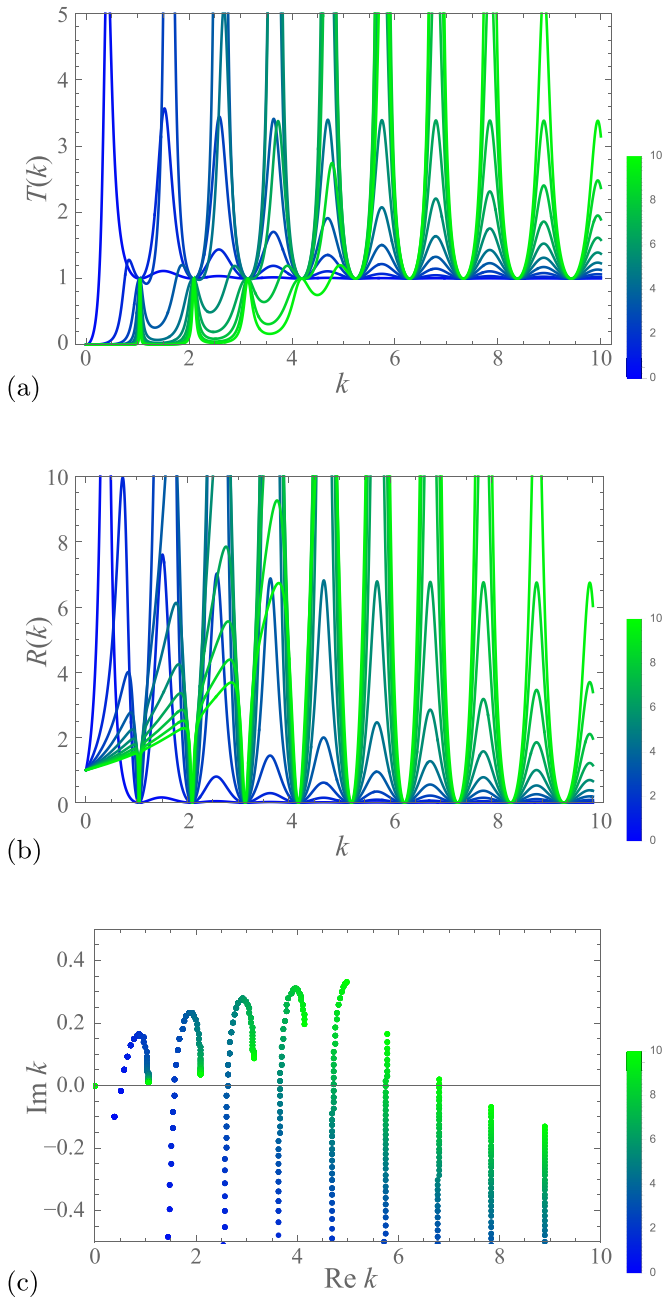
FIG. 8. Variation of (a) the transmission probability $T(k)$ and (b) the reflection probability $R(k)$ with $\gamma/|t_h|$ varied from 0 to 10 at $\tilde{L} = 3$. (c) The corresponding trajectories of discrete eigenvalues in the complex k plane. The color bars show the value of $\gamma/|t_h|$.

peaks is $\Delta k = \pi/\tilde{L} \simeq 1$. Figure 8(c) shows the trajectories of the discrete eigenvalues. We can understand the features from the ones in Figs. 4 and 6 as follows. We can regard the dispersion relation of the continuum model, namely $E(k) = \hbar^2 k^2/(2m) = |t_h| a^2 k^2$, as the leading term of the expansion of the lattice dispersion $E(k) = -2|t_h| \cos ka$ with respect to the small parameter a except for the constant shift $-2|t_h|$. In this sense, the low-energy region of the continuum model is a magnification of the low-energy limit of the lattice model. Therefore, what happens in Fig. 8 magnifies what happens in the left half of each panel of Fig. 4 with many more peaks.

We can thus see that for a fixed range of k, $T(k)$ and $R(k)$ diverge when the corresponding eigenvalue crosses the real axis for a relatively small value of $\tilde{\gamma}$. Then they turn to the Fabry-Pérot-type behavior when the corresponding eigenvalue turns and comes back toward the real axis. As a result, we observe the following:

(i) A Fabry-Pérot region appears in the range $k < \tilde{\gamma}/2$.

(ii) Divergent peaks appear in the intermediate range $k > \tilde{\gamma}/2$.

(iii) In the regime of $k \gg \tilde{\gamma}/2$, i.e., at $k \to \infty$, one recovers a unitary but trivial behavior. $T(k) = 1$ and $R(k) = 0$.

In the Fabry-Pérot regime, $k < \tilde{\gamma}/2$, the peaks appear when

$$e^{2ik\tilde{L}} = 1, \tag{69}$$

i.e., at $k = n\pi/\tilde{L}$ ($n = 1, 2, \dots$), while in the intermediate regime, the divergence occurs at

$$e^{2ik\tilde{L}} = -1, \tag{70}$$

i.e., at

$$k = k^{(n)} = \frac{(2n-1)\pi}{2\tilde{L}} \quad (n = 1, 2, \dots) \tag{71}$$

and at the value of $\tilde{\gamma}$ such that

$$\tilde{\gamma} = \sqrt{2} k^{(n)}. \tag{72}$$

VI. CONCLUDING REMARKS

We have considered the non-Hermitian scattering problem for a Fabry-Pérot-type PT-symmetric model. We found that both the transmission and reflection probabilities, $T(k)$ and $R(k)$, behave strongly atypically with divergent peaks in the regime of weak non-Hermiticity, $\gamma < 2|t_h|$, while the behavior of $T(k)$ becomes superficially Hermitian in the regime of strong non-Hermiticity, $\gamma > 2|t_h|$. In the latter, $T(k)$ shows conventional Fabry-Pérot peaks that are bounded by unity, i.e., $T(k) \leqslant 1$ as in the Hermitian case, and yet the behavior of $R(k)$ is unconventional, leading to breaking the unitarity of the S-matrix: $T^2 + R^2 \neq 1$. We exactly obtained the expressions for the transmission and reflection coefficients $\mathcal{T}(k)$ and $\mathcal{R}(k)$ by simply summing the Fabry-Pérot infinite series. By interpreting this formula, we have clarified the reason why $T(k)$ and $R(k)$ drastically change their behavior at $\gamma = 2|t_h|$.

One may wonder whether such a peculiar Fabry-Pérot-type feature in the transmission probability can be observed in a purely lossy experiment. The idea of a passive PT-symmetric system is based on the fact that adding a constant (here chosen to be $-i\gamma$ with $\gamma > 0$) to all sites in the system leaves the system exactly the same, and by doing so the system would become more easily realized in an experiment without a balanced gain. In the case of the two-site PT-symmetric model discussed in the Introduction, this principle works out successfully; the behavior of the exceptional point in the gain-loss model is successfully reproduced in a passive model with the diagonal elements of the Hamiltonian shifted to 0 and $-2i\gamma$.

In an infinite system that we consider here, however, performing literally the same operation, i.e., adding $-i\gamma$ to all sites, seems impossible. Instead, one may think of adding $-i\gamma$ only to the two potential sites. However, this breaks the PT-symmetry. The exact Fabry-Pérot feature with transmission

peaks of height 1 (corresponding to the perfect transmission) is unique to the PT-symmetric gain-loss setup. When the strength of gain and loss potentials is not perfectly balanced, namely when the PT-symmetry is weakly broken, one can still see Fabry-Pérot-type resonant peaks, but the peaks become either higher or lower than 1.

We have discussed in Sec. II a related but still different case of the single on-site imaginary scatterer as a tutorial example. In this prototypical example, the behavior of the transmission probability $T(E)$ sharply changes at the exceptional point specified at $\gamma = 2|t_h|$, from a pair of sharp divergent peaks for $\gamma < 2|t_h|$ [Fig. 2(a)] to a finite, broadened peak structure for $\gamma > 2|t_h|$ [Fig. 2(b)]. This drastic change in $T(E)$ corresponds to the shift of the eigenvalues; they are initially located on the real axis in the complex energy plane for $\gamma < 2|t_h|$, they collide at the exceptional point, and they turn into the imaginary axis for $\gamma > 2|t_h|$ [see Fig. 2(c)]. In this example, we have pointed out that by reversing the sign of the hopping amplitude t_h, one can effectively (i.e., as far as the behavior of the transmission and reflection coefficients is concerned) convert a loss to a gain, and by doing so a divergent peak in the transmission probability becomes accessible in a purely lossy experiment.

In the PT-symmetric model, on the other hand, there seems to be no such apparent correspondence between the colliding eigenvalues in the complex k plane and the change of the behavior in $T(k)$ and $R(k)$. Also, in a strict sense the characteristic non-Hermitian Fabry-Pérot feature described in Secs. III and IV is realized only in the case of a single non-Hermitian site on each side, i.e., only at sites 0 and L. In the case of more than one non-Hermitian site on each side, one can still see the remnants of the Fabry-Pérot feature found in the case above, but the peaks become narrower and their heights are no longer strictly smaller than 1. The behavior of discrete eigenvalues under the Siegert boundary condition is also susceptible to the number of non-Hermitian sites. Still, the Fabry-Pérot regime exists in the continuum limit, where we find a crossover to the regime of divergent transmission peaks.

To summarize, in a strict sense the non-Hermitian Fabry-Pérot feature is realized only in the limit of extremely thin non-Hermitian scatterers with PT symmetry, but a tendency toward this characteristic limit may be visible in more realistic potential setups.

APPENDIX A: DISCRETE EIGENVALUES OF OPEN QUANTUM SYSTEMS UNDER THE SIEGERT BOUNDARY CONDITION

Once we carry out the analytic continuation of the transmission and reflection coefficients (27) and (29) on the

complex k plane, we find poles, which are often termed resonance poles. In fact, one of the textbook definitions of resonance is a pole of the S-matrix, but we can also define it as an eigenstate of the Schrödinger equation under a specific boundary condition.

Since the transmission and reflection coefficients have the denominator A, their poles are given by the zeros of A [64]. This means that the wave functions at the resonance poles are given by setting A to zero in Eq. (21), that is,

$$\psi_x = \begin{cases} Be^{-ikx} & \text{for } x \leqslant 0, \\ Ce^{ikx} & \text{for } x \geqslant L. \end{cases} \tag{A1}$$

This wave function contains outgoing waves only for $\mathrm{Re}\,k > 0$ and incoming waves only for $\mathrm{Re}\,k < 0$, which is called the Siegert boundary condition [60] for the wave functions of discrete eigenvalues; see Ref. [65] for a summary.

In fact, the solutions include all kinds of discrete states with point spectra, namely bound states, antibound states, resonant states, and antiresonant states. To give an example, the wave function of the form (A1) is a bound state if k is a pure imaginary number with a positive imaginary part. In the standard Hermitian scattering problem with time-reversal symmetry, the solutions on the positive imaginary axis are the bound states as exemplified above, those on the negative imaginary axis are called the antibound states, those in the fourth quadrant of the complex k plane are the resonant states, and those in the third quadrant are called the antiresonant states, which are the time-reversal states of the resonant states. (In addition, there are continuum states on the real axis.) States on the upper half of the complex k plane are prohibited except on the positive imaginary axis because of the normalization [64]. For non-Hermitian problems, however, it is known that the poles can move across the real axis of the complex k plane [44].

In the specific example of the model (20), we obtain the eigenvalue equation for the Siegert boundary condition (A1) by setting $\tilde{A}$ to zero in Eq. (33), and therefore the discrete eigenvalues are the solutions of $\det M_L = 0$, which we find from Eq. (B10):

$$4t_h^2 \sin^2 k - \gamma^2(e^{2ikL} - 1) = 0. \tag{A2}$$

This is none other than the equation for the zeros of the denominator of $\mathcal{T}(k)$ and $\mathcal{R}(k)$ in Eqs. (27) and (29).

For numerical calculations of the discrete eigenvalues, however, finding all solutions of the nonlinear equation (A2) is generally not easy. We briefly review here a convenient method of numerically finding the discrete eigenvalues; see Ref. [60] for details. The eigenvalue equation to be solved reads

$$\begin{pmatrix} i\gamma + t_h e^{ik} & t_h & & & \\ t_h & & t_h & & \\ & t_h & & \ddots & \\ & & \ddots & & t_h \\ & & & t_h & -i\gamma + t_h e^{ik} \end{pmatrix} \vec{\psi}(k) = E\vec{\psi}(k). \tag{A3}$$

This is a nonlinear eigenvalue problem because the left-hand side is a function of the eigenvalue E through the wave number $k = \arccos[E/(2t_h)]$.

More specifically, we can cast it into a second-order eigenvalue problem with respect to $\beta = e^{ik}$. Using this variable, we transform Eq. (A3) to

$$(\beta^2 U + \beta V + W)\vec{\psi}(\beta) = 0, \tag{A4}$$

where

$$U = -t_{\mathrm{h}} I_{L+1} + t_{\mathrm{h}} \begin{pmatrix} 1 & & & & \\ & 0 & & & \\ & & \ddots & & \\ & & & 0 & \\ & & & & 1 \end{pmatrix}, \tag{A5}$$

$$V = \begin{pmatrix} i\gamma & t_{\mathrm{h}} & & & \\ t_{\mathrm{h}} & & t_{\mathrm{h}} & & \\ & t_{\mathrm{h}} & & \ddots & \\ & & \ddots & & t_{\mathrm{h}} \\ & & & t_{\mathrm{h}} & -i\gamma \end{pmatrix}, \tag{A6}$$

$$W = -t_{\mathrm{h}} I_{L+1}. \tag{A7}$$

We can further transform this into a generalized but linear eigenvalue equation by doubling the vector space as follows [60,66]:

$$\begin{pmatrix} \beta I_{L+1} & -I_{L+1} \\ W & \beta U + V \end{pmatrix} \begin{pmatrix} \vec{\psi}(\beta) \\ \beta \vec{\psi}(\beta) \end{pmatrix} = 0, \tag{A8}$$

which is a $(2L + 2)$-dimensional matrix equation. The $(L + 1)$-dimensional first row of Eq. (A8) guarantees that the second row of the vector is always β-fold its first row. The second row of the equation is equivalent to Eq. (A4).

Equation (A8) is a linear eigenvalue equation with respect to β in the sense that

$$\begin{pmatrix} 0 & I_{L+1} \\ -W & -V \end{pmatrix} \begin{pmatrix} \vec{\psi}(\beta) \\ \beta \vec{\psi}(\beta) \end{pmatrix} = \beta \begin{pmatrix} I_{L+1} & 0 \\ 0 & U \end{pmatrix} \begin{pmatrix} \vec{\psi}(\beta) \\ \beta \vec{\psi}(\beta) \end{pmatrix}. \tag{A9}$$

We can numerically find the $2(L + 1)$ pieces of eigenvalues for small L easily. Note, however, that because the $(1,1)$ and $(L + 1, L + 1)$ elements of U are missing, we in fact find only $2L$ pieces of eigenvalues in the present case. To find full eigenvalues, we should introduce modulation of the hopping amplitudes on the left and right edges of the scattering region $[0, L]$; see Appendix H of Ref. [67].

APPENDIX B: ANALYTIC EXPRESSIONS OF THE TRANSMISSION AND REFLECTION PROBABILITIES

We invert the matrix M_L in Eq. (35) and obtain the formulas (27) and (29) from the expressions (39) and (40). The (i, j) element of the inverse matrix M_L^{-1} is given by

$$\left(M_L^{-1}\right)_{ij} = (-1)^{i+j} \frac{\det M_L^{ji}}{\det M_L}, \tag{B1}$$

where $\det M_L^{ji}$ is the cofactor of M_L, that is, the determinant of an $L \times L$ matrix M_L^{ji} that we make from the $(L + 1) \times (L + 1)$ matrix M_L by removing the jth row and the ith column. To write down the expressions (39) and (40) explicitly, we therefore need $\det M_L$ as well as the cofactors $\det M_L^{1,L+1}$ and $\det M_L^{1,1}$.

We can find the determinant of the matrix M_L in Eq. (35) by cofactor expansion. For brevity of notation, let us fix $L = 4$ for

the moment. The cofactor expansion with respect to the first row gives

$$\det M_4 = (i\gamma - t_{\mathrm{h}} e^{-ik})$$

$$\times \det \begin{pmatrix} -E(k) & t_{\mathrm{h}} & & \\ t_{\mathrm{h}} & -E(k) & t_{\mathrm{h}} & \\ & t_{\mathrm{h}} & -E(k) & t_{\mathrm{h}} \\ & & t_{\mathrm{h}} & -i\gamma - t_{\mathrm{h}} e^{-ik} \end{pmatrix}$$

$$- t_{\mathrm{h}}^2 \det \begin{pmatrix} -E(k) & t_{\mathrm{h}} & \\ t_{\mathrm{h}} & -E(k) & t_{\mathrm{h}} \\ & t_{\mathrm{h}} & -i\gamma - t_{\mathrm{h}} e^{-ik} \end{pmatrix}. \tag{B2}$$

The further cofactor expansion with respect to the last row gives

$$\det M_4 = (i\gamma - t_{\mathrm{h}} e^{-ik})(-i\gamma - t_{\mathrm{h}} e^{-ik})$$

$$\times \det \begin{pmatrix} -E(k) & t_{\mathrm{h}} & \\ t_{\mathrm{h}} & -E(k) & t_{\mathrm{h}} \\ & t_{\mathrm{h}} & -E(k) \end{pmatrix}$$

$$- (i\gamma - t_{\mathrm{h}} e^{-ik})t_{\mathrm{h}}^2 \det \begin{pmatrix} -E(k) & t_{\mathrm{h}} \\ t_{\mathrm{h}} & -E(k) \end{pmatrix}$$

$$- t_{\mathrm{h}}^2(-i\gamma - t_{\mathrm{h}} e^{-ik}) \det \begin{pmatrix} -E(k) & t_{\mathrm{h}} \\ t_{\mathrm{h}} & -E(k) \end{pmatrix}$$

$$+ t_{\mathrm{h}}^4 \det (-E(k)). \tag{B3}$$

This algebra for $L = 4$ implies the general expression

$$\det M_L$$

$$= \left(\gamma^2 + t_{\mathrm{h}}^2 e^{-2ik}\right) d_{L-1} + 2t_{\mathrm{h}}^3 e^{-ik} d_{L-2} + t_{\mathrm{h}}^4 d_{L-3}, \tag{B4}$$

where d_n denotes the determinant of $n \times n$ matrix with all the diagonal elements $-E(k) = -t_{\mathrm{h}}(e^{ik} + e^{-ik})$ and all super- and subdiagonal elements t_{h}.

We can find d_n again by cofactor expansion to obtain the recurrence equation

$$d_n = -t_{\mathrm{h}}(e^{ik} + e^{-ik}) d_{n-1} - t_{\mathrm{h}}^2 d_{n-2}. \tag{B5}$$

The solutions of the characteristic equation for the recurrence equation (B5), $\xi^2 + 2\xi t_{\mathrm{h}} \cos k + t_{\mathrm{h}}^2 = 0$, are $\xi = -t_{\mathrm{h}} e^{\pm ik}$, and hence we have

$$d_n + t_{\mathrm{h}} \beta d_{n-1} = -t_{\mathrm{h}} \beta^{-1} (d_{n-1} + t_{\mathrm{h}} \beta d_{n-2})$$

$$= (-t_{\mathrm{h}})^{n-2} \beta^{-n+2} (d_2 + t_{\mathrm{h}} \beta d_1)$$

$$= (-t_{\mathrm{h}})^n \beta^{-n}, \tag{B6}$$

where $\beta = e^{ik}$. Transforming this to

$$\frac{d_n \beta^n}{(-t_{\mathrm{h}})^n} = \beta^2 \frac{d_{n-1} \beta^{n-1}}{(-t_{\mathrm{h}})^{n-1}} + 1 \tag{B7}$$

gives

$$\frac{d_n \beta^n}{(-t_{\mathrm{h}})^n} + \frac{1}{\beta^2 - 1} = \beta^2 \left[\frac{d_{n-1} \beta^{n-1}}{(-t_{\mathrm{h}})^{n-1}} + \frac{1}{\beta^2 - 1} \right]$$

$$= \beta^{2(n-1)} \left(\frac{d_1 \beta}{-t_{\mathrm{h}}} + \frac{1}{\beta^2 - 1} \right)$$

$$= \frac{\beta^{2(n+1)}}{\beta^2 - 1}, \tag{B8}$$

and hence

$$d_n = (-t_{\mathrm{h}})^n \frac{\beta^{n+2} - \beta^{-n}}{\beta^2 - 1} = (-t_{\mathrm{h}})^n \frac{\sin(n+1)k}{\sin k}. \quad (\mathrm{B}9)$$

Substituting this into Eq. (B4), we finally arrive at

$$\det M_L = (-t_{\mathrm{h}})^{L+1} \left[\tilde{\gamma}^2 \frac{\beta^L - \beta^{-L}}{\beta - \beta^{-1}} - \beta^{-L}(\beta - \beta^{-1}) \right]$$

$$= (-t_{\mathrm{h}})^{L+1} \left(\tilde{\gamma}^2 \frac{\sin kL}{\sin k} - 2ie^{-ikL} \sin k \right), \quad (\mathrm{B}10)$$

where $\tilde{\gamma} = \gamma / t_{\mathrm{h}}$.

Let us next compute the cofactors $\det M_L^{1,L+1}$ and $\det M_L^{1,1}$. The easier one is the former,

$$\det M_L^{1,L+1} = t_{\mathrm{h}}^L. \quad (\mathrm{B}11)$$

The slightly more complicated one is the latter. By cofactor expansion, we have

$$\det M_L^{1,1} = (-i\gamma - t_{\mathrm{h}}\beta^{-1}) d_{L-1} - t_{\mathrm{h}}^2 d_{L-2}$$

$$= (-t_{\mathrm{h}})^L \left(i\tilde{\gamma} \frac{\beta^L - \beta^{-L}}{\beta - \beta^{-1}} + \beta^{-L} \right)$$

$$= (-t_{\mathrm{h}})^L \left(i\tilde{\gamma} \frac{\sin kL}{\sin k} + e^{-ikL} \right). \quad (\mathrm{B}12)$$

Summarizing the results (B10)–(B12), we arrive at the two elements of the inverted matrix that we need as follows:

$$\left(M_L^{-1} \right)_{L+1,1} = (-1)^{L+2} \frac{\det M_L^{1,L+1}}{\det M_L}$$

$$= \frac{-2ie^{ikL}t_{\mathrm{h}} \sin k}{4t_{\mathrm{h}}^2 \sin^2 k + \gamma^2(e^{2ikL} - 1)}, \quad (\mathrm{B}13)$$

$$\left(M_L^{-1} \right)_{1,1} = \frac{\det M_L^{1,1}}{\det M_L}$$

$$= \frac{-2it_{\mathrm{h}} \sin k - i\gamma(e^{2ikL} - 1)}{4t_{\mathrm{h}}^2 \sin^2 k + \gamma^2(e^{2ikL} - 1)}. \quad (\mathrm{B}14)$$

Inserting these into Eqs. (39) and (40), we arrive at the same expressions as Eqs. (27) and (29).

---

[1] Y. Ashida, Z. Gong, and M. Ueda, Non-Hermitian physics, arXiv:2006.01837.

[2] R. E. Le Levier and D. S. Saxon, An optical model for nucleon-nuclei scattering, Phys. Rev. **87**, 40 (1952).

[3] H. Feshbach, C. E. Porter, and V. F. Weisskopf, Model for nuclear reactions with neutrons, Phys. Rev. **96**, 448 (1954).

[4] P. E. Hodgson, The neutron optical potential, Rep. Prog. Phys. **47**, 613 (1984).

[5] H. Feshbach, Unified theory of nuclear reactions, Ann. Phys. **5**, 357 (1958).

[6] H. Feshbach, A unified theory of nuclear reactions. II, Ann. Phys. **19**, 287 (1962).

[7] H.-P. Breuer, E.-M. Laine, J. Piilo, and B. Vacchini, Colloquium: Non-Markovian dynamics in open quantum systems, Rev. Mod. Phys. **88**, 021002 (2016).

[8] S. Diehl, A. Micheli, A. Kantian, B. Kraus, H. P. Büchler, and P. Zoller, Quantum states and phases in driven open quantum systems with cold atoms, Nat. Phys. **4**, 878 (2008).

[9] W. R. Frensley, Boundary conditions for open quantum systems driven far from equilibrium, Rev. Mod. Phys. **62**, 745 (1990).

[10] H.-P. Breuer and F. Petruccione, in *The Theory of Open Quantum Systems* (Oxford University Press, Oxford, 2007), p. 656.

[11] N. Hatano and D. R. Nelson, Localization Transitions in Non-Hermitian Quantum Mechanics, Phys. Rev. Lett. **77**, 570 (1996).

[12] N. Hatano and D. R. Nelson, Non-Hermitian delocalization and eigenfunctions, Phys. Rev. B **58**, 8384 (1998).

[13] J. Feinberg and A. Zee, Non-Hermitian random matrix theory: Method of Hermitian reduction, Nucl. Phys. B **504**, 579 (1997).

[14] J. Feinberg and A. Zee, Non-Gaussian non-Hermitian random matrix theory: Phase transition and addition formalism, Nucl. Phys. B **501**, 643 (1997).

[15] J. T. Chalker and B. Mehlig, Eigenvector Statistics in Non-Hermitian Random Matrix Ensembles, Phys. Rev. Lett. **81**, 3367 (1998).

[16] C. M. Bender and S. Boettcher, Real Spectra in Non-Hermitian Hamiltonians Having PT Symmetry, Phys. Rev. Lett. **80**, 5243 (1998).

[17] C. M. Bender, D. C. Brody, and H. F. Jones, Complex Extension of Quantum Mechanics, Phys. Rev. Lett. **89**, 270401 (2002).

[18] K. G. Makris, R. El-Ganainy, D. N. Christodoulides, and Z. H. Musslimani, Beam Dynamics in $\mathcal{PT}$ Symmetric Optical Lattices, Phys. Rev. Lett. **100**, 103904 (2008).

[19] R. El-Ganainy, K. G. Makris, D. N. Christodoulides, and Z. H. Musslimani, Theory of coupled optical PT-symmetric structures, Opt. Lett. **32**, 2632 (2007).

[20] S. Klaiman, U. Günther, and N. Moiseyev, Visualization of Branch Points in $\mathcal{PT}$-Symmetric Waveguides, Phys. Rev. Lett. **101**, 080402 (2008).

[21] A. Guo, G. J. Salamo, D. Duchesne, R. Morandotti, M. Volatier-Ravat, V. Aimez, G. A. Siviloglou, and D. N. Christodoulides, Observation of $\mathcal{PT}$-Symmetry Breaking in Complex Optical Potentials, Phys. Rev. Lett. **103**, 093902 (2009).

[22] C. E. Rüter, K. G. Makris, R. El-Ganainy, D. N. Christodoulides, M. Segev, and D. Kip, Observation of parity–time symmetry in optics, Nat. Phys. **6**, 192 (2010).

[23] A. Regensburger, C. Bersch, M.-A. Miri, G. Onishchukov, D. N. Christodoulides, and U. Peschel, Parity–time synthetic photonic lattices, Nature (London) **488**, 167 (2012).

[24] H. Hodaei, M.-A. Miri, M. Heinrich, D. N. Christodoulides, and M. Khajavikhan, Parity-time–symmetric microring lasers, Science **346**, 975 (2014).

[25] L. Feng, Z. J. Wong, R.-M. Ma, Y. Wang, and X. Zhang, Single-mode laser by parity-time symmetry breaking, Science **346**, 972 (2014).

[26] K. Esaki, M. Sato, K. Hasebe, and M. Kohmoto, Edge states and topological phases in non-Hermitian systems, Phys. Rev. B **84**, 205128 (2011).

[27] Y. C. Hu and T. L. Hughes, Absence of topological insulator phases in non-Hermitian *PT*-symmetric Hamiltonians, Phys. Rev. B **84**, 153101 (2011).

[28] Z. Gong, Y. Ashida, K. Kawabata, K. Takasan, S. Higashikawa, and M. Ueda, Topological Phases of Non-Hermitian Systems, Phys. Rev. X **8**, 031079 (2018).

[29] K. Kawabata, K. Shiozaki, M. Ueda, and M. Sato, Symmetry and Topology in Non-Hermitian Physics, Phys. Rev. X **9**, 041015 (2019).

[30] H. Schomerus, Topologically protected midgap states in complex photonic lattices, Opt. Lett. **38**, 1912 (2013).

[31] C. Yuce, Topological phase in a non-Hermitian PT symmetric system, Phys. Lett. A **379**, 1213 (2015).

[32] C. Poli, M. Bellec, U. Kuhl, F. Mortessagne, and H. Schomerus, Selective enhancement of topologically induced interface states in a dielectric resonator chain, Nat. Commun. **6**, 6710 (2015).

[33] S. Weimann, M. Kremer, Y. Plotnik, Y. Lumer, S. Nolte, K. G. Makris, M. Segev, M.-C. Rechtsman, and A. Szameit, Topologically protected bound states in photonic parity–time-symmetric crystals, Nat. Mater. **16**, 433 (2017).

[34] M. A. Bandres, S. Wittek, G. Harari, M. Parto, J. Ren, M. Segev, D. N. Christodoulides, and M. Khajavikhan, Topological insulator laser: Experiments, Science **359**, 1231 (2018).

[35] T. E. Lee, Anomalous Edge State in a Non-Hermitian Lattice, Phys. Rev. Lett. **116**, 133903 (2016).

[36] S. Yao and Z. Wang, Edge States and Topological Invariants of Non-Hermitian Systems, Phys. Rev. Lett. **121**, 086803 (2018).

[37] K. Yokomizo and S. Murakami, Non-Bloch Band Theory of Non-Hermitian Systems, Phys. Rev. Lett. **123**, 066404 (2019).

[38] K.-I. Imura and Y. Takane, Generalized bulk-edge correspondence for non-Hermitian topological systems, Phys. Rev. B **100**, 165430 (2019).

[39] K.-I. Imura and Y. Takane, Generalized Bloch band theory for non-Hermitian bulk-boundary correspondence, Prog. Theor. Exp. Phys. **2020**, 12A103 (2020).

[40] L. Xiao, X. Zhan, Z. H. Bian, K. K. Wang, X. Zhang, X. P. Wang, J. Li, K. Mochizuki, D. Kim, N. Kawakami, W. Yi, H. Obuse, B. C. Sanders, and P. Xue, Observation of topological edge states in parity-time-symmetric quantum walks, Nat. Phys. **13**, 1117 (2017).

[41] R. Landauer, Spatial variation of currents and fields due to localized scatterers in metallic conduction, IBM J. Res. Dev. **1**, 223 (1957).

[42] Z. Lin, H. Ramezani, T. Eichelkraut, T. Kottos, H. Cao, and D. N. Christodoulides, Unidirectional Invisibility Induced by $\mathcal{PT}$-Symmetric Periodic Structures, Phys. Rev. Lett. **106**, 213901 (2011).

[43] S. Longhi, Invisibility in PT-symmetric complex crystals, J. Phys. A **44**, 485302 (2011).

[44] S. Garmon, M. Gianfreda, and N. Hatano, Bound states, scattering states, and resonant states in $\mathcal{PT}$-symmetric open quantum systems, Phys. Rev. A **92**, 022125 (2015).

[45] L. Moreno-Rodríguez, F. Izrailev, and J. Méndez-Bermúdez, PT-symmetric tight-binding model with asymmetric couplings, Phys. Lett. A **384**, 126495 (2020).

[46] O. Vázquez-Candanedo, F. Izrailev, and D. Christodoulides, Spectral and transport properties of the PT-symmetric dimer model, Physica E **72**, 7 (2015).

[47] C. M. Bender, Introduction to PT-symmetric quantum theory, Contemp. Phys. **46**, 277 (2005).

[48] W. D. Heiss, The physics of exceptional points, J. Phys. A **45**, 444016 (2012).

[49] Y. D. Chong, L. Ge, H. Cao, and A. D. Stone, Coherent Perfect Absorbers: Time-Reversed Lasers, Phys. Rev. Lett. **105**, 053901 (2010).

[50] A. Mostafazadeh, Spectral Singularities of Complex Scattering Potentials and Infinite Reflection and Transmission Coefficients at Real Energies, Phys. Rev. Lett. **102**, 220402 (2009).

[51] A. Mostafazadeh, Resonance phenomenon related to spectral singularities, complex barrier potential, and resonating waveguides, Phys. Rev. A **80**, 032711 (2009).

[52] A. Mostafazadeh, Optical spectral singularities as threshold resonances, Phys. Rev. A **83**, 045801 (2011).

[53] S. Longhi, Spectral singularities in a non-Hermitian Friedrichs-Fano-Anderson model, Phys. Rev. B **80**, 165125 (2009).

[54] S. Longhi, Spectral singularities and Bragg scattering in complex crystals, Phys. Rev. A **81**, 022102 (2010).

[55] C. M. Bender and T. T. Wu, Anharmonic oscillator, Phys. Rev. **184**, 1231 (1969).

[56] P. E. Shanley, Spectral singularities of the quartic anharmonic oscillator, Phys. Lett. A **117**, 161 (1986).

[57] W. Wan, Y. Chong, L. Ge, H. Noh, A. D. Stone, and H. Cao, Time-reversed lasing and interferometric control of absorption, Science **331**, 889 (2011).

[58] S. Longhi, Coherent perfect absorption in a homogeneously broadened two-level medium, Phys. Rev. A **83**, 055804 (2011).

[59] A. J. F. Siegert, On the derivation of the dispersion formula for nuclear reactions, Phys. Rev. **56**, 750 (1939).

[60] N. Hatano and G. Ordonez, Time-reversal symmetric resolution of unity without background integrals in open quantum systems, J. Math. Phys. **55**, 122106 (2014).

[61] N. Hatano, Equivalence of the effective hamiltonian approach and the siegert boundary condition for resonant states, Fortschr. Phys. **61**, 238 (2013).

[62] G. Breit and E. Wigner, Capture of slow neutrons, Phys. Rev. **49**, 519 (1936).

[63] See Supplemental Material at http://link.aps.org/supplemental/10.1103/PhysRevResearch.3.013223 for the evolution of $T(k)$ [video 1 (case of $L = 7$), video 2 (case of $L = 6$)], and for the evolution of discrete eigenvalues in the complex k-plane (video 3).

[64] L. D. Landau and L. M. Lifshitz, *Quantum Mechanics Non-Relativistic Theory*, 3rd ed. (Butterworth-Heinemann, Oxford, 1981), Sec. 134.

[65] N. Hatano, K. Sasada, H. Nakamura, and T. Petrosky, Some properties of the resonant state in quantum mechanics and its computation, Prog. Theor. Phys. **119**, 187 (2008).

[66] F. Tisseur and K. Meerbergen, The quadratic eigenvalue problem, SIAM Rev. **43**, 235 (2001).

[67] K. Sasada, N. Hatano, and G. Ordonez, Resonant spectrum analysis of the conductance of an open quantum system and three types of fano parameter, J. Phys. Soc. Jpn. **80**, 104707 (2011).